Çukurova Üniversitesi Mühendislik Mimarlık Fakültesi Dergisi, 35(4), ss. 1073-1081, Aralık 2020
Çukurova University Journal of the Faculty of Engineering and Architecture, 35(4), pp. 1073-1081, December 2020

Antibacterial and Optical Properties of Mn Doped ZnO Nanopowders Synthesized via Spray Drying and Subsequent Thermal Decomposition

Şeyma DUMAN[*1], Büşra BULUT[1], Burak ÖZKAL[2]

[1]*Bursa Technical University, Metallurgical and Materials Engineering Department, Bursa*
[2]*Istanbul Technical University, Metallurgical and Materials Engineering Department, Istanbul*

Geliş tarihi: 28.10.2020 Kabul tarihi: 30.12.2020

Abstract

Mn doped ZnO nanopowders with homogenous particle distribution were synthesized using spray drying and thermal decomposition dual methods. Synthesis was carried out in spray drying slurry containing zinc acetate powders followed by calcining the as-prepared powders at 300, 400, and 500^{o}C. Mn doping was achieved by adding manganese (II) acetate at different concentrations between 0.01-0.05 M during the synthesis. The obtained powders were characterized by a variety of characterization techniques. The results of phase analysis revealed that Mn-doped ZnO nanopowders having a single hexagonal structured ZnO phase. According to the results of microstructural and UV-vis characterizations; morphologies and optical properties of the Mn-doped ZnO nanopowders were affected by Mn doping. Furthermore, the results of this study exhibited that the addition of Mn have a significant influence on the antibacterial performance of the synthesized ZnO nanopowders.

Keywords: Mn doped ZnO, Spray drying, Optical properties, Antibacterial properties

Püskürtmeli Kurutma ve Ardından Termal Bozunma ile Sentezlenen Mn Katkılı ZnO Nanotozların Antibakteriyel ve Optik Özellikleri

Öz

Homojen dağılımlı Mn katkılı ZnO nanotozlar, püskürtmeli kurutma ve termal bozunma ikili yöntemleri kullanılarak sentezlenmiştir. Sentez, çinko asetat tozları içeren püskürtmeli kurutma bulamacında gerçekleştirilmiş olup, ardından hazırlanan tozlar 300, 400 ve 500^{o}C'de kalsine edimiştir. Sentez sırasında 0,01-0,05 M arasında farklı konsantrasyonlarda mangan (II) asetat ilave edilerek Mn katkısı sağlanmıştır. Elde edilen tozların karalterizasyonu gerçekleştirilmiştir. Faz analizinin sonuçları, Mn katkılı ZnO nanotozlarının, altıgen bir yapıda tek bir ZnO fazına sahip olduğunu ortaya çıkardı. Mikroyapısal ve UV-görünür karakterizasyon sonuçlarına göre Mn katkısı, ZnO nanotozlarının morfolojilerini ve optik özelliklerini değiştirmiştir. Ayrıca sonuçlar, Mn ilavesinin sentezlenmiş ZnO nanotozların antibakteriyel performansını önemli ölçüde artırabildiğini ortaya koymuştur.

Anahtar Kelimeler: Mn katkılı ZnO, Püskürtmeli kurutma, Optik özellikler, Antibakteriyel özellikler

[*]Sorumlu yazar (Corresponding author): Şeyma DUMAN, *seyma.duman@btu.edu.tr*

1. INTRODUCTION

ZnO is an important material due to its low cost, environment-friendly, high stability property, and high optical transparency thanks to its direct large bandgap (3.37 eV) and high binding energy (60 meV) [1,2]. By doping the transition metals (Fe, Mn, Co, Cr, Ni) into ZnO, the properties of ZnO nanostructures can be altered like the shape and size of the nanoparticles, and its optical, antibacterial, electrical, and magnetic properties can be enhanced [2,3]. Transition metals doped ZnO, especially manganese (Mn), is a promising functional material with good optic, ferromagnetic, photocatalytic activity, and antibacterial properties due to the fact that new energy situation within the bandgap of ZnO is generated by Mn^{+2} doping [4]. So, it can be used for applications including optoelectronics, solar cells, varistors, high performance, and biomedical sensors [4,5]. Furthermore, Mn-doped ZnO nanoparticles display strong absorption in the UV visible range [6,7]. It was reported by Ma and Wang [7] who found that while particle size decreased, the absorbance of UV light increased. Venkataprasad Bhat and Deepak were also reported that increasing calcination temperature was increased the particle size of nanoparticles [6,8]. According to studies in the literature, when Mn concentration into ZnO is increased, the optical band gap and particle size of nanopowders decrease [6,9].

Various methods have been studied for obtaining Mn-doped ZnO nanopowders such as hydrothermal, solvothermal, sol-gel, and chemical vapor deposition [6,10-12]. Synthesis of Mn-doped ZnO nanopowders which has homogeneous dispersed can be difficult with only a thermal decomposition process by using acetate-based powders [13,14]. Therefore, spray drying, which is transformed from feed slurry to dry homogeneous granules by spraying into a hot medium, was performed as a preliminary process [13-15]. The preparation of anode material for lithium-ion batteries was successfully carried out by spray drying and subsequent thermal decomposition [16].

The present study reports the synthesis of Mn-doped ZnO particles during thermal decomposition of spray dried manganese acetate doped zinc acetate-based granules. The effect of various Mn dopant concentrations and different thermal decomposition temperatures were investigated. The characterization of the ultimate powders was conducted using by scanning electron microscopy (SEM), energy dispersive spectroscopy (EDS), nano-particle size distribution (Nano-PSD), specific surface area measurement (BET), X-ray diffractometer (XRD), UV-vis. spectroscopy, true, and apparent density measurements. The antibacterial performance of the nanocomposites was investigated. The results showed that the addition of Mn can significantly improve the antibacterial performance of the synthesized nanocomposites with also improving their optical properties.

2. MATERIAL AND METHOD

2.1. Fabrication Procedure

Zinc acetate dihydrate ($Zn(CH_3COO)_2.2H_2O$) Alfa Aesar^{TM}), manganese acetate tetrahydrate ($Mn(CH_3COO)_2.4H_2O$ Alfa Aesar^{TM}) all in powder form were used as starting materials. Aqueous solutions of 1 M zinc acetate (hereafter $Zn(Ac)_2$) were prepared by dissolving it in 50 ml distilled water. For the preparation of doped samples, 0.01, 0.02, 0.03, 0.04, or 0.05 M manganese acetate (hereafter $Mn(Ac)_2$) was added into the zinc acetate solution and stirred to obtain homogeneous solutions at room temperature for 30 minutes. Prepared five different solutions were spray dried prior to thermal decomposition using a laboratory-scale spray dryer. Spray drying conditions such as inlet temperature, feed rate, and drying air flow rate were adjusted 220^{o}C, 3 ml/min and 800 ml/min, respectively. Also, these experiments were spray dried by using on Büchi brand Mini Spray-Dryer B-290. 2 g of the spray dried powders were placed in an alumina crucible and later placed in a furnace. The crucible was heated to 300°C, 400°C and 500°C with a heating rate of 2°C/min in air atmosphere and held for 12 h dwell time at

peak temperature. The flow chart summarizes the experimental details given in Figure 1.

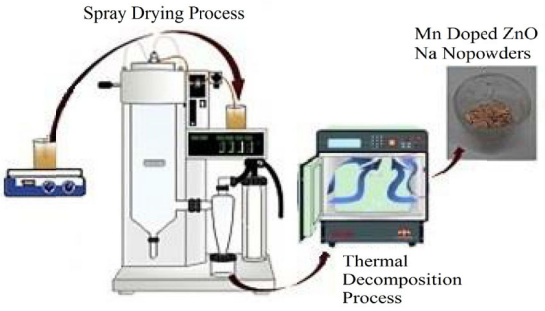

Figure 1. The flow chart showing the applied procedure for prepared samples.

Scanning electron microscopy (FE-SEM, Quanta^{TM} FEG 250) and energy-dispersive spectroscopy (EDS) characterized the morphology of the synthesized Mn-doped ZnO nanopowders. X-ray diffraction (XRD, Bruker^{TM} D8 Advance) analyses were performed on the crystal structures using Cu oK radiation in a scanning range from 20^{o} to 80^{o} with a step size of 2°/min on the 2θ. Particle size measurements of the powders were conducted using Microtrac^{TM} Stabino Particle Size Distribution. The specific surface area of the synthesized nanopowders prepared in this study was measured using the Brunauer–Emmett–Teller (BET) method via Quantachrome^{TM} Autosorb-1 MP device. For this purpose, all samples were outgassed for at least 3 h at 120 °C prior to the adsorption measurements. The apparent and true densities were measured with Arnold density measurement kit and helium pycnometer (Micromeritics^{TM}, Accupyc 1330), respectively. The optical absorbance of the synthesized powders was determined by a Shimadzu^{TM} UVmini-1240 UV-vis Spectrophotometer in the wavelength range between 200 and 800 nm.

Antibacterial activity tests were performed with Staphylococcus aureus (S. aureus), yeast and mold ATCC 6538 and ATCC) suspensions of microorganisms in a pH 7 Maximum Recovery Diluent according to ASTM 2149 method. Also, Model bacteria Escherichia coli (E. coli), which is yeast and mold (ATCC 35218) suspensions of microorganism, was tested with different nanocomposites in the same method. Nanocomposites were weighed as 1 g and placed in a 250 mL flask with 50 mL of microorganism solution. The sealed flasks were shaken at 37 ^{o}C in an incubator, and solution samples were collected after 10 minutes, 20 minutes, and 30 minutes of contact times. Serial dilutions of the solutions contacting the surfaces were plated on Muller-Hinton II agar and incubated for a duration of 24 h and a temoerature of 37 ^{o}C. The presence of viable bacteria was determined by Colony counts.

3. RESULTS AND DISCUSSION

In our previous studies [13,14], it was reported the synthesis of ZnO nanoparticles by spray drying and subsequent thermal decomposition processes as a result of the decomposition reaction of zinc acetate into ZnO. In this study, the same processes were used and Mn-doped ZnO was synthesized by using manganese acetate tetrahydrate as a dopant material and compared with ZnO nanopowders synthesized previously.

Figure 2 shows FE-SEM micrographs of the spray dried powders and the synthesized Mn-doped ZnO nanopowders. It is clear that spherical granules were obtained after spray drying of zinc acetate based solution (Figure 2a). We observed similar granulation behavior for the Mn-doped ZnO nanopowders as well. During thermal decomposition of zinc acetate to ZnO, new nanoparticles were created by destroying spray dried spherical granules. It is determined in the previous study that a characteristic morphology was not observed after the thermal decomposition of zinc acetate in the absence of dopants [14]. It is shown in Figure 2b-d that rod-shaped morphology was achieved in the presence of Mn dopant after the thermal decomposition process, but this morphology has an irregular structure. Because of Mn doping, the length, and diameter of rod-shaped ZnO nanoparticles increases in comparison to the undoped one. It was previously found reported in the article by Panda et. al [17] that the diameter and length of Mn-doped ZnO nanorods showed a slight increase comparing to the undoped ZnO nanorods. It is very clear that dopants play a key role in the change of morphology.

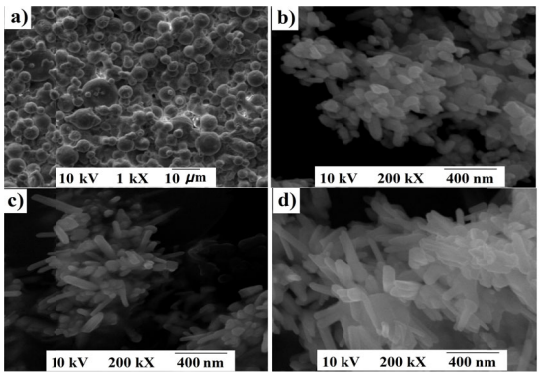

Figure 2. SEM micrographs of the synthesized Mn doped ZnO nanopowders: a) Spray dried zinc acetate powders, b) Z-1M, c) Z-3M and d) Z-5M

The physical properties of powders after thermal decomposition process are summarized in Table 1. While the particle sizes for undoped and Mn doped ZnO nanopowders were between the range of 235-306 nm. It was observed that with Mn doping and the increase of dopant concentrations, particle size was decreased whereas the BET surface area was increased in the range of 18.50- 28.04 m^2/g. The theoretical density of ZnO is 5.61 g/cm^3. Apparent and true densities of the synthesized Mn doped ZnO nanopowders are given in Table 1. While the apparent density values for undoped and Mn doped ZnO nanopowders decreased from 0.25 g/cm^3 to 0.18 g/cm^3, true density values increased from 5.58 g/cm^3 to 5.62 g/cm^3. The theoretical density of Mn is 7.21 g/cm^3 and when Mn incorporated into ZnO, true density values were increased. Mn doped ZnO nanopowders displayed poor flow and packing characteristics due to the formation of rod-like and irregular structures; therefore, apparent density values decrease.

Table 1. Physical properties of the synthesized Mn doped ZnO nanopowders

Sample	Particle Size (nm)	Specific surface area (m^2/g)	Length /Diameter (L/D)	Apparent Density (g/cm^3)	True Density (g/cm^3)
Z	306	18.50	2.5	0.25±0.03	5.58±0.05
Z-1M	298.8	25.40	2.6	0.23±0.01	5.58±0.06
Z-2M	295.7	25.48	-	0.22±0.03	5.59±0.02
Z-3M	292.1	25.57	3.1	0.20±0.07	5.60±0.05
Z-4M	290.3	26.63	-	0.20±0.06	5.61±0.09
Z-5M	289	28.04	3.5	0.18±0.09	5.62±0.01

Z-5M sample synthesized at 300°C was selected due to its high density and synthesized at 400°C and 500°C for investigating the effect of different temperatures. SEM micrographs of the synthesized Z-5M nanopowders at different temperatures were shown in Figure 3. It can be observed from Figure 3 that the morphologies of the Mn doped ZnO changes greatly with an increase in temperature. Thermal decomposition at temperatures higher than 500°C led to having in thicker rod-diameter and shorter rod-length of the nanoparticles. Toloman et. al. [18] reported that the morphology is clearly improved when the temperature increases.

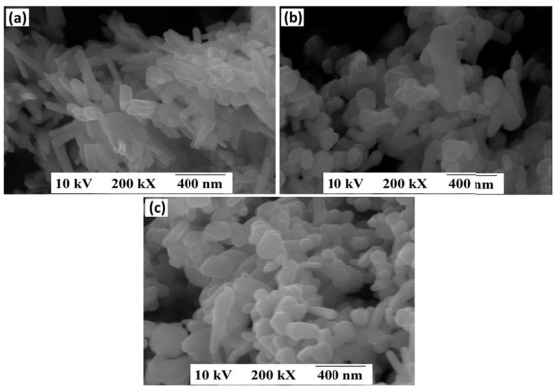

Figure 3. SEM micrographs of the synthesized Z-5M nanopowders at different temperatures: a) 300 °C, b) 400 °C and c) 500 °C.

The density results of the synthesized Z-5M nanopowders at different temperatures are tabulated in Table 2. In this table, it can be noticed a decrease in apparent density with increasing the thermal decomposition temperature. Furthermore, the true density of Z-5M nanopowders, determined as 5.62 g/cm^3, increased with increasing of temperature and was measured as 5.65 g/cm^3.

Table 2. Density results of the synthesized Z-5M nanopowders at different temperatures

Temperature (^{o}C)	Apparent Density (g/cm^3)	True Density (g/cm^3)
300	0.18±0.09	5.62±001
400	0.16±0.04	5.63±0.014
500	0.11±0.03	5.65±0.02

Figure 4a presents the XRD patterns of Mn doped ZnO nanopowders by thermal decomposition of the spray dried powders. It was confirmed in the XRD patterns that the peaks of ZnO have crystalline quality and peaks position are in good agreement with standard JCPDS card no. 70-8070 [14]. The high-density peaks corresponding to the planes (100), (002), and (101) are clear evidence of the formation of the hexagonal structure of ZnO. No other peaks corresponding to Mn related secondary or impurity phase was found in Mn-doped ZnO nanopowders. This situation was commented in the literature as the incorporation of Mn ion into the Zn lattice site [19]. Furthermore, peaks intensity of Mn doped ZnO nanopowders increased with increasing of Mn concentration.

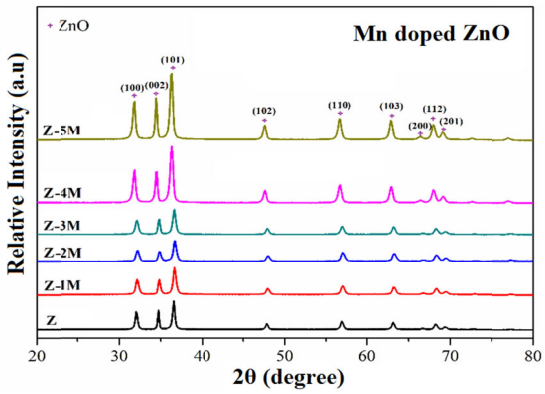

(a)

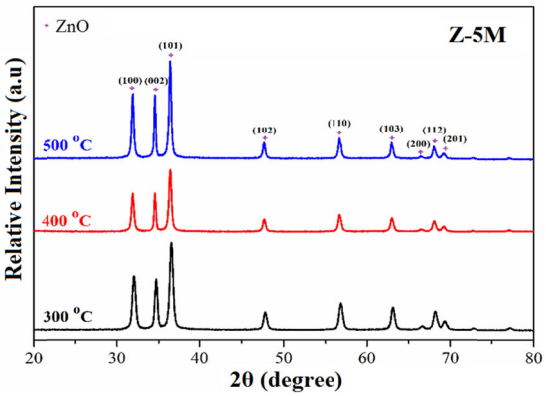

(b)

Figure 4. XRD patterns of the synthesized nanopowders by thermal decomposition of the spray dried powders: a) Mn doped ZnO and b) Z-5M synthesized at different temperatures

Figure 4b shows the XRD patterns of the Z-5M nanopowders synthesized by thermal decomposition at different temperatures of the spray dried powders. While thermal decomposition temperature increased to 400 ^{o}C and 500 ^{o}C, crystalline quality increased and all the diffraction peaks were in accordance with the JCPDS card no. 70-8070. Except for ZnO characteristic peaks, no extra peaks which can be composed of manganese clusters, zinc or their complex oxides could be detected. These results are in good agreement with those obtained by Ahmed [20].

The average crystallite sizes of undoped and Mn-doped ZnO nanopowders are estimated from the full width at half maximum (FWHM) of the XRD peaks using Debye-Scherrer's equation as follows:

$$D = \frac{k\lambda}{\beta \cos\theta} \qquad (1)$$

where β is the corrected half-peak width of the experimental sample (FWHM), θ is Bragg angle, λ = is the X-ray wavelength (1.54˚A), and k is the shape factor of value 0.9. The mean crystallite sizes of the samples synthesized in different Mn concentrations are given in Table 3. The XRD patterns show a slight shift in the peaks of the high concentration of Mn doping compared to undoped

ZnO nanopowders. According to Table 3, the mean crystalline size of the undoped and Mn-doped ZnO nanopowders is in the range of 22.7–28.1 nm. The small grain growth of Mn doped ZnO as compare to pure ZnO nanoparticles resulted in a decrease in the mean crystallite size when Mn doping in ZnO crystal increases. Mote et al. [5] also reported quite parallel mean crystallite size for Mn-doped ZnO samples. The mean crystallite sizes of the Z-5M sample synthesized in different thermal decomposition temperature are given in Table 4. Using the plane (101) (main peak) for Z-5M nanopowders, the crystallite size was found to increase in this thermal decomposition range (Table 4). ZnO crystallite size increased from 22.7 nm for the Z-5M sample thermally decomposed at 300°C to 26.4 and 31.3 nm for Z-5M samples thermally decomposed at 400 and 500°C. However, the XRD patterns show slight in the peaks of Z-5M with an increase in temperature.

Table 3. XRD results of undoped and Mn doped ZnO nanopowders

Mn concentration (M)	(101), 2θ (°C)	D (nm)	Lattice parameters	
			a (A°)	c (A°)
0	36.871	28.1	3.2496	5.2065
1	36.832	27.8	3.2501	5.2069
3	36.778	25.9	3.2510	5.2088
5	36.615	22.7	3.2519	5.2094

Table 4. XRD results of Z-5M nanopowders synthesized at different temperatures

Temperature (°C)	(101), 2θ (°C)	D (nm)	Lattice parameters	
			a (A°)	c (A°)
300	36.615	22.7	3.2519	5.2094
400	36.587	26.4	3.2498	5.2019
500	36.413	31.3	3.2432	5.1911

Effect of dopant and temperature on optical properties of the synthesized samples by thermal decomposition of the spray dried powders was determined by UV-vis Spectrophotometric analysis at room temperature. Figure 5 shows optical absorption spectra of Mn doped ZnO nanopowders in the visible range prepared by synthesizing in different Mn concentration and thermally decomposing at various temperatures.

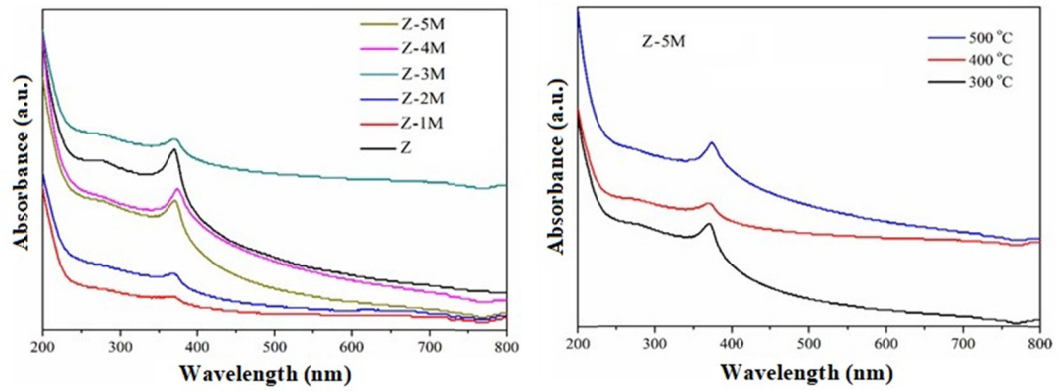

(a) **(b)**

Figure 5. UV-vis spectroscopy of the synthesized samples: (a) Mn doped ZnO in different concentrations and (b) Z-5M sample in different temperatures

In the previous study, a single and the characteristic band peaking of undoped ZnO nanopowders was indicated at 375 nm [14]. It can be seen from Figure 5a that the absorption peak of Mn doped ZnO get shifted towards higher energy values compared to undoped ZnO. This situation shows that optical properties in the visible region improve with Mn doping. Our UV-vis results are in agreement with Li et al. [21] reported enhancing optical properties while the sample color is darker. Figure 5b shows the optical absorption spectra of Z-5M nanopowders in the visible range thermally decomposed at various temperatures. The thermally decomposed Z-5M nanopowders at different temperatures revealed the increase in the intensity of the 381 nm peak (the characteristic peak of wurzite structure of ZnO) increases with the increase of the decomposition temperature. The resulting Z-5M nanorods exhibited enhanced optical properties even after thermal decomposition at high temperatures.

Antibacterial activities of ZnO and Mn doped ZnO nanopowders synthesized at 300^{o}C are shown in Table 5. Our study aimed to develope the antibacterial properties of ZnO nanopowders by Mn addition. According to antibacterial activity results in Table 5, the antibacterial activity of the Mn doped ZnO granules is impressed regardless of dependent on the type of bacteria in both gram-positive and gram-negative bacteria. Mn doped ZnO nanopowders had stronger antibacterial activity against the Gram-positive bacterium S. aureus than against the Gram-negative bacterium E. coli. Moreover, the antibacterial properties of Z-5M nanopowders increased with decreasing crystallite size.

Table 5. Antibacterial activities of ZnO and Mn doped ZnO nanopowders synthesized at 300^{o}C

Samples	Concentrations (mg/L)	D (nm)	Zone of inhibition (ZOI) (mm)	
			E. coli	S. aureus
Z	50	28.1	21	23
Z-3M	50	25.9	23	25
Z-5M	50	22.7	26	29

4. CONCLUSIONS

The effects of the dopant concentration and thermal decomposition temperature on the morphology of the Mn doped ZnO nanopowders synthesized via spray drying and subsequent thermal decomposition processes have been investigated in the present study. Based on the obtained results, the following conclusions can be drawn:

1. Microstructural characterizations by SEM revealed that new ZnO nanoparticles have rod-like structures, were created by destroying spray dried zinc acetate spherical granules. It is very clear that dopant and temperature play a key role in morphology changing.
2. The Mn doping was increased true densities, as the particle sizes of ZnO decreased. The temperature was also increased the true densities of Mn doped ZnO nanopowder.
3. From XRD investigations result that the Mn doped ZnO for the analyzed samples increases with the decrease of the Mn concentration. Contrary to this, the crystallite size for the analyzed samples increases with the increase of the thermal decomposition temperature.
4. As a result of our investigations, it seems that the optical properties in Mn doped ZnO nanopowders gave similar results with those low-temperature thermally decomposed samples. Furthermore, the optical properties in the Z-5M sample enhanced after thermally treated at high temperatures.
5. The antibacterial activity is enhanced for Mn doped ZnO nanopowders by Mn doping.

5. ACKNOWLEDGE

This work is supported by ITU-BAP 36459 project.

6. REFERENCES

1. Ozgur U., Alivov Y.I., Liu C., Take A., Reshchikov M.A., Dogan S., Avrutin V., Cho S.J., Markoc H., 2005. A Comprehensive Review of ZnO Materials and Devices, Journal of Applied Physics, 98, 041301.

2. Khosravi-Gandomani S., Yousefi R., Jamali-Sheini F., Huang N.M., 2014. Optical and Electrical Properties of P-type Ag-doped ZnO Nanostructures, Ceramics International, 40, 7957-7963.

3. Yousefi, R., Jamli-Sheini, F., 2012. Effect of Chlorine Ion Concentration on Morphology and Optical Properties of Cl-doped ZnO Nanostructures, Ceramics International, 38(7), 5821-5825.

4. Ravichandran, K., Karthika, K., Sakthivel, B., Jabena Begum, N., Snega, S., Swaminathan, K., Senthamilselvi, V., 2014. Tuning the Combined Magnetic and Antibacterial Properties of ZnO Nanopowders Through Mn Doping for Biomedical Applications, Journal of Magnetism and Magnetic Materials, 358-359, 50–55.

5. Mote, V.D., Dargad, J.S., Purushotham, Y., Dole, B.N., 2015. Effect of Doping on Structural, Physical, Morphological and Optical Properties of $Zn_{1-x}Mn_xO$ Nano-particles, Ceramics International, 41, 15153–15161.

6. Omri, K., El, Ghoul, J., Lemine, O.M., Bououdina, M., Zhang, B., El Mira, L., 2013. Magnetic and Optical Properties of Manganese Doped ZnO Nanoparticles Synthesized by Sol–gel Technique, Superlattices and Microstructures 60, 139–147.

7. Ma, X., Wang, Z., 2011. The UV and Blue Light Emission Properties of Mn Doped ZnO Nanocrystals, Microelectronic Engineering, 88(10), 3168-3171.

8. Bhat, S.V., Deepak, F.L., 2005. Tuning the Bandgap of ZnO by Substitution with Mn^{2+}, Co^{2+} and Ni^{2+}, Solid State Communications, 135(6), 345-347.

9. Senthilkumaar, S., Rajendran, K., Banerjee, S., Chinic, T.K., Sengodan, V., 2008. Influence of Mn Doping on the Microstructure and Optical Property of ZnO, Materials Science in Semiconductor Processing, 11(1) 6-12.

10. Vethanathan, S.J.K., Brightson, M., Sundar, S.M., Perumal, S., 2011. Synthesis of Mn Doped ZnO Nanocrystals by Solvothermal Route and its Characterization, Materials Chemistry and Physics, 125, 872–875.

11. Jiang, Y.J., Wang, W., Jing, C.B., Cao, C.Y., Chu, J.H., 2011. Sol-gel Synthesis, Structure and Magnetic Properties of Mn-doped ZnO Diluted Magnetic Semiconductors, Materials Science and Engineering: B 176, 1301–1306.

12. Yan, H.L., Wang, J.B., Zhong, X.L., 2011. Zn-catalyzed Growth Processes and Ferromagnetism of Mn-doped ZnO Nanorods on Si Substrate, Applied Surface Science, 257, 5017–5020.

13. Duman, Ş., Ozkal, B., 2016. Powder State Characterization of ZnO/C and NiO/C Composite Nanopowders Synthesized Via Spray Drying Subsequent Thermal Decomposition, XIII. International Congress Winter Session 'Machines, Technologies, Materials' (MTM 2016), 14-17 September 2016, Varna – Bulgaria, 36-39.

14. Duman, Ş., Ozkal, B., 2016. Effect of Dopant and Binder on the Formation of ZnO Powders During Thermal Decomposition of Spray Dried Zinc-acetate Based Granules, Journal of Optoelectronics and Advanced Materials, 18, 705-711.

15. Bertrand, G., Roy, P., Filiatre, V., Coddet, C., 2005. Spray-dried Ceramic Powders: A Quantitative Correlation Between Slurry Characteristics and Shapes of the Granules, Chemical Engineering Science, 60, 95-102.

16. Lin, B., Wen, Z.Y., Gu, Z.H., Huang, S.H., 2008. Morphology and Electrochemical Performance of $Li[Ni_{1/3}Co_{1/3}Mn_{1/3}]O_2$ Cathode Material by a Slurry Spray Drying Method, Journal of Power Sources, 175, 564-569.

17. Panda, J., Sasmal, I., Nath, T.K., 2016. Magnetic and Optical Properties of Mn-doped ZnO Vertically Aligned Nanorods Synthesized by Hydrothermal Technique, AIP Advances, 6, 035118-10.

18. Toloman, D., Mesaros, A., Popa, A., Raita, O., Silipas, T.D., Vasile, B.S., Pana, O., Giurgiu, L.M., 2013. Evidence by EPR of

Ferromagnetic Phase in Mn-doped ZnO Nanoparticles Annealed at Different Temperatures, Journal of Alloys and Compounds. 551, 502–507.

19. Urbieta, A., Fernández, P., Piqueras, J., 2012. Nanowires and Stacks of Nanoplates of Mn Doped ZnO Synthesized by Thermal Evaporation-deposition, Materials Chemistry and Physics, 132, 1119–1124.

20. Ahmed, S.A., 2017. Structural, Optical, and Magnetic Properties of Mn-doped ZnO Samples, Results in Physics, 7, 604–610.

21. Li, W., Wang, G., Chen, C., Liao, J., Li, Z., 2017. Enhanced Visible Light Photocatalytic Activity of ZnO Nanowires Doped with Mn^{2+} and Co^{2+} Ions, Nanomaterials 7, 1-11.